J. Fluid Mech. (2000), *vol.* 420, *pp.* 1–25. Printed in the United Kingdom

© 2000 Cambridge University Press

Temporal instability of compound threads and jets

By A. CHAUHAN[1], C. MALDARELLI[1]†, D. T. PAPAGEORGIOU[2] AND D. S. RUMSCHITZKI[1]†

[1]The Levich Institute and Department of Chemical Engineering, City College of CUNY, 140th Street and Convent Avenue, New York, NY 10031, USA

[2]Department of Mathematics, Center for Applied Mathematics and Statistics, New Jersey Institute of Technology, Newark, NJ 07102, USA

(Received 27 May 1999 and in revised form 17 April 2000)

Compound threads and jets consist of a core liquid surrounded by an annulus of a second immiscible liquid. Capillary forces derived from axisymmetric disturbances in the circumferential curvatures of the two interfaces destabilize cylindrical base states of compound threads and jets (with inner and outer radii R_1 and aR_1 respectively). The capillary instability causes breakup into drops; the presence of the annular phase allows both the annular- and core-phase properties to influence the drop size. Of technological interest is breakup where the core snaps first, and then the annulus. This results in compound drops. With jets, this pattern can form composite particles, or if the annular fluid is evaporatively removed, single drops whose size is modulated by both fluids.

This paper is a study of the linear temporal instability of compound threads and jets to understand how annular fluid properties control drop size in jet breakup, and to determine conditions which favour compound drop formation. The temporal dispersion equation is solved numerically for non-dimensional annular thicknesses a of order one, and analytically for thin annuli ($a - 1 = \epsilon \ll 1$) by asymptotic expansion in ϵ. There are two temporally growing modes: a stretching mode, unstable for wavelengths greater than the undisturbed inner circumference $2\pi R_1$, in which the two interfaces grow in phase; and a squeezing mode, unstable for wavelengths greater than $2\pi aR_1$, which grows exactly out of phase. Growth rates are always real, indicating that in jetting configurations disturbances convect downstream with the base velocity. For order-one thicknesses, the growth rate of the stretching mode is higher for the entire range of system parameters examined. The drop size scales with the wavenumber of the maximally growing wave (k_{max}). We find that for the dominant stretching mode and $a = 2$, variations from 0.1 to 10 in the ratios of the annulus to core viscosity, or the tension of the outer surface to that of the inner interface, can result in changes in k_{max} by a factor of approximately 2. However, for these changes in the system ratios, the growth rate (s_{max}) and the ratio of the amplitude of the outer to the inner interface (A_{max}) for the fastest growing wave only change marginally, with A_{max} near one. The system appears most sensitive to the ratio of the density of the annulus to the core fluid. For a variation between 0.1 and 10, k_{max} again changes by a factor of 2, but A_{max} and s_{max} vary more significantly with large amplitude ratios for low density ratios. The amplitude ratio of the stretching mode at the maximally growing wave (A_{max}) indicates whether the film or core will break first. When this ratio is near one, linear theory predicts that the core breaks with the

† Authors to whom the correspondence should be addressed.

https://doi.org/10.1017/S0022112000001282 Published online by Cambridge University Press

annulus intact, forming compound drops. Except for low values of the density ratio, our results indicate that most system conditions promote compound drop formation.

For thin annuli, the growth rate disparity between modes becomes even greater. In the limit $\epsilon \to 0$, the squeezing growth rate is roughly proportional to ϵ^2 while the stretching mode growth rate is roughly proportional to ϵ^0 and asymptotes to a single jet with radius R_1 and tension equal to the sum of the two tensions. Thus, in this limit the growth rate and k_{max} are independent of the film density and viscosity. The amplitude ratio of the stretching mode becomes equal to one for all wavenumbers; so thin films break as compound drops. Our results compare favourably with previously published measurements on unstable waves in compound jets.

1. Introduction

Axisymmetric circumferential capillary forces destabilize a liquid thread. Rayleigh (1879) analysed the temporal instability of a static, doubly infinite, inviscid thread of radius R_1, density ρ and tension σ by imposing a monochromatic interfacial disturbance of wavenumber q and k (real) in the θ- and z-directions, respectively, at $t = 0$, and examining its time evolution with normal modes $\exp(\mathrm{i}(kz+q\theta)+s(k,q)t)$, $s(k,q) = s_r + \mathrm{i}s_i$, where s_r is the temporal growth rate and $-s_i/k$ the wave speed. The balance between the destabilizing circumferential curvature and the stabilizing axial curvature is such that axisymmetric ($q = 0$) waves longer than the undisturbed jet circumference grow ($s_r > 0$) without travelling ($s_i = 0$), those shorter and/or non-axisymmetric decay, and there exists a wavelength $k_{max} = 0.697/R_1$ of maximal instability. Since the instability is capillary-driven, consideration of fluid viscosity (Chandrasekhar 1961), and of an infinite, immiscible surrounding fluid (Tomotika 1935) do not change the qualitative picture; viscosity lowers growth rates and elongates the fastest growing wave.

The temporal linear stability of a static thread applies to liquid bridge collapse in microgravity and the setting of thin-walled annular polymer moulds, but its main application is to the breakup into drops of jets emerging from a nozzle tip. Examples of the latter occur in ink jet printing (cf. the review by Kamphoefner 1972), fuel injection, particle sorting (Hertzberg, Sweet & Herzberg 1976) and polymer fibre spinning (Denn 1980). In jets, disturbances generally arise at the nozzle tip and, for a uniformly convecting base state, one would expect them to simply convect with the jet velocity $V(s_i(k) = -kV)$ while growing ($s_r > 0$). However, since these disturbances arise continuously in time (and not just at $t = 0$) at $z = 0$, Keller, Rubinow & Tu (1973) suggested that a spatial analysis for the harmonic response $\exp(\mathrm{i}k(\omega)z + \mathrm{i}\omega t)$ ($s = \pm\mathrm{i}\omega$ imaginary; $k = k(s(\omega)) = k_r + \mathrm{i}k_i$ complex; k_r the wavelength, k_i the spatial growth rate), was more appropriate. They found that for Weber numbers $W = \rho V^2 R_1/\sigma > 3.2$ and non-dimensional frequencies (Strouhal numbers) $\omega R_1/V$ between zero and a cutoff depending on W, but close to 1, disturbances grow axially. If the linear theory holds until close to breakup, the k with the largest negative imaginary part can predict drop size ($\sim 1/k_r(\omega)$) and the distance $z(\sim 1/k_i(\omega))$ from the nozzle to breakup. For asymptotically large W, disturbances do in fact simply convect with the base velocity ($k_r(\omega) = \omega/V$) and grow with the temporal growth rate ($k_i(\omega) = -s_r(k_r)/V$) and the temporal analysis predicts the same drop sizes and breakup lengths as the (linear) convective theory. For $W < 3.2$, the jet becomes absolutely unstable and grows both in space and in time due to a pinch singularity in the dispersion equation (Leib & Goldstein 1986*a*). The critical W increases with

https://doi.org/10.1017/S0022112000001282 Published online by Cambridge University Press

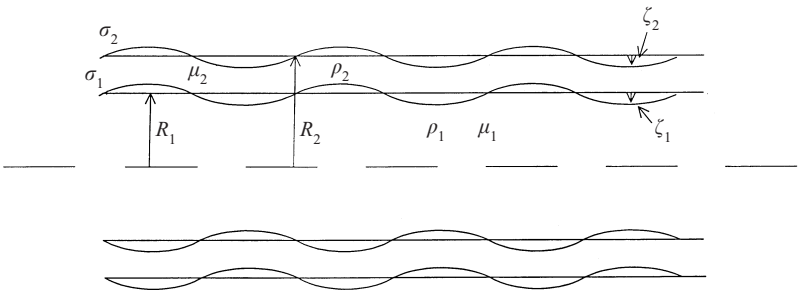


FIGURE 1. Geometry of the compound jet.

inclusion of the density of the surrounding fluid (Lin & Lian 1989) and, if one includes viscosity (Leib & Goldstein 1986*b*), with increasing Reynolds numbers $Re := \rho V R_1/\mu$.

A large body of experiments (see e.g. Donnelly & Glaberson 1966; Goedde & Yuen 1970; Rutland & Jameson 1970, 1971; Lafrance 1975; Taub 1976; Pimbley & Lee 1977; Chaudhary & Maxworthy 1980*a*; Bousfield, Stockel & Nanivadekar 1990 and the reviews by McCarthy & Molloy 1974; Bogy 1979; Yarin 1993; Eggers 1997) apply a sinusoidal periodic disturbance of frequency ω at the nozzle tip to study capillary jet breakup into drops. These studies, usually at sufficiently high Weber numbers to be in the asymptotically large W regime, with $k_r = \omega/V$, and $k_i V = -s_r(k_r)$, follow the inviscid predictions almost to breakup. They show that when the disturbances imposed at the nozzle tip are sufficiently large, nonlinear coupling of other harmonics also only enter near breakup. The fine structure at the point of breakup, including necking and satellite formation under both jetting and low-velocity dripping conditions (where jets do not form but pendant shapes emerge, neck and detach from a nozzle), has been the subject of several further experimental studies (Pimbley & Lee 1977; Chaudhary & Maxworthy 1980*b*; Peregrine, Shoker & Symon 1990; Vassallo & Ashgriz 1991; Shi, Brenner & Nagel 1994; Basaran & Zhang 1995; Kowalewski 1996; Clanet & Lasheras 1999). Theoretical efforts, including a series of weakly nonlinear (Wang 1968; Yuen 1968; Nayfeh 1970; Lafrance 1975; Chaudhary & Redekopp 1980; Busker, Lamers & Nieuwenhuizen 1989), fully nonlinear numerical (Mansour & Lundgren 1990; Tjahjadi, Stone & Ottino 1992; Zhang & Stone 1997; Zhang 1999) and nonlinear one-dimensional or slender body studies (Lee 1974; Pimbley 1976; Bogy 1978; Bogy, Shine & Talke 1980; Bousfield & Denn 1987; Wilson 1988; Ting & Keller 1990; Eggers 1993; Schulkes 1993; Brenner, Shi & Nagel 1994; Eggers & Dupont 1994; Bechtel, Carlson & Forest 1995; Eggers 1995; Brenner *et al.* 1997), have captured some of the details of the breakup.

This paper is a study of the capillary-driven linear instability of compound threads and jets composed of two immiscible fluids: fluid 1 in a circular core and fluid 2 in a surrounding concentric annulus (figure 1). Fluid properties and other parameters are subscripted with the fluid number. Applications of compound and simple jets are similar, including ink jet printing (Hertz & Hermanrud 1983), but the former also include the formation of compound fibres and particles. Having a second fluid and a second destabilizing interface in a compound jet introduce additional physical parameters that one can manipulate to control size and the breakup length. Alternatively viewed, compound jets are a link between liquid films and liquid jet problems.

Sanz & Masseguer (1985) and Radev & Shkadov (1985) performed one-dimensional (pressure and velocity only functions of z) temporal analyses of inviscid compound jets for axisymmetric disturbances and found two growing modes. One, with the larger

https://doi.org/10.1017/S0022112000001282 Published online by Cambridge University Press

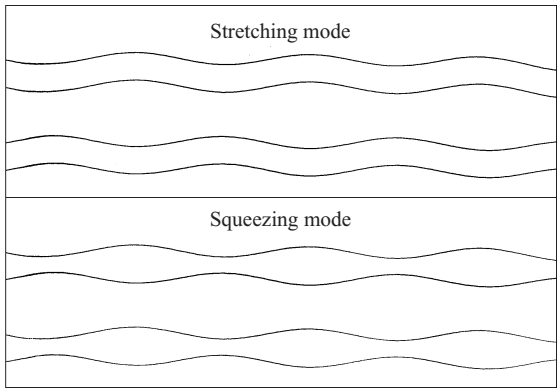


FIGURE 2. The stretching and the squeezing modes.

growth rate, is a stretching (ST) mode (both interfaces move in phase) driven by capillary forces at the inner surface R_1, and the other is a squeezing (SQ) mode (interfaces exactly out of phase) driven by the capillary forces at the outer interface. See figure 2. Inclusion of viscosity and radial motions (Radev & Tchavdarov 1988 and Shkadov & Sisoev 1996) do not qualitatively change these features. They allow study of the effects of the outer-to-inner ratios d, m, γ of respectively density, viscosity and surface tension on the growth rate s_r, its maximum s_{max} and corresponding wavenumber k_{max}, and on the amplitude ratio A_{max} of the outer-to-inner interfacial disturbances, the latter being useful in determining whether the core or the film breaks first.

Radev & Tchavdarov (1988) and Shkadov & Sisoev (1996) do not provide systematic calculations of k_{max} or s_{max} as a function of the system ratios. More importantly, few calculations are presented for A_{max} at k_{max} for the dominant stretching mode. This is important in determining how the compound jet breaks up, assuming linear theory is applicable to breakup and the jet is subject to a wide enough disturbance to realize this wavenumber. Radev & Tchavdarov (1988) find the distance to the first breakup point is the minimum of L_1 and L_2, where $L_1 := [V/s_{r(ST)}(k_{max})] \ln (R_1/\xi_1)$ corresponds to core breakup first, and $L_2 := [V/s_{r(ST)}(k_{max})] \ln ((R_2 - R_1)/(|\xi_2 - \xi_1|))$ corresponds to the annulus breaking first, where ξ_1 and ξ_2 are the amplitudes of the inner and outer interfaces, respectively, at $z = 0$. The former is ideal for composite drop production since it leads to drops of core liquid in a continuous jet of annular fluid, and then to composite drops as the outer interface snaps-off. Initial film snap-off can be problematic for composite drop formation unless the annular liquid rapidly wets the core fluid after the core finally breaks. Conditions under which $A_{max} \approx 1$ are those favouring composite formation and knowledge of how m, d and γ control A_{max} would technologically be quite instructive. Radev & Tchavdarov (1988) provide only a dependence on γ, while Sanz & Masseguer (1985)'s more complete study is for their one-dimensional, inviscid model.

The above studies examine temporal instability. Chauhan *et al.* (1996) presented the axisymmetric spatial instability of a compound inviscid jet, and found two spatially unstable modes: one, with the larger growth rate, unstable for dimensionless frequencies (Strouhal numbers $\omega R_1/V$) between 0 and 1, and a second unstable between 0 and R_1/R_2. They extended Keller *et al.*'s (1973) large W asymptotic which supports the usefulness of the temporal analysis to compound jets. Given its relevance at high W, we now examine the temporal stability of an axisymmetric compound, viscous thread with the following goals, as differentiated from those already in the

https://doi.org/10.1017/S0022112000001282 Published online by Cambridge University Press

literature: (i) We shall carry out a detailed study of the dependences of s_{max} and k_{max} on m, d and γ to see how to use the annular fluid to tune drop size and breakup distances. Radev & Tchavdarov (1988) and Shkadov & Sisoev (1996) non-dimensionalize using the base velocity V and their stability curves depend on Re and W. Since the base velocity only convects the instability, the growth rate is a function only of $\boldsymbol{J}(\boldsymbol{J} = \rho_1 R_1 \sigma_1/\mu_1^2 = Re^2/W)$ and not of Re and W independently, as a static thread. We make this change. (ii) We present a detailed study of A_{max} of the maximally growing wave as a function of the system ratios to predict the breakup sequence. (iii) We will analytically examine the thin-annular-film $(R_2 - R_1)/R_1 = \epsilon \ll 1$ limit for the growth rates. This analysis is not only applicable to thin-film applications, but also sheds light on the physics of each of the unstable modes and their parameter dependences. We also develop long-wave results ($k \to 0, \epsilon = O(1)$), which serve as the starting point for the weakly nonlinear evolution of the instability (Papageorgiou, Maldarelli & Rumschitzki 1990), and is useful in validating numerical calculations.

2. Formulation of the linear stability

A doubly infinite thread of a fluid of density ρ_1 and viscosity μ_1 is surrounded by a coaxial annulus of an immiscible fluid of density ρ_2 and of viscosity μ_2. Both fluids are assumed incompressible. In the base state there is no flow, and the interfaces are cylindrical and concentric with inner and outer radii R_1 and R_2. The tensions of the inner and outer interfaces are σ_1 and σ_2, respectively (cf. figure 1). In the stationary base state the pressure distribution is given by

$$p_2^{[0]} = \gamma/a, \quad p_1^{[0]} = 1 + \gamma/a, \tag{1}$$

where $p_i^{[0]}$ denotes the base-state non-dimensional pressure of region $i(i = 1$ is the core, $i = 2$ is the annular domain and the superscript [0] denotes the base state), pressure is scaled with the capillary pressure $[\sigma_1/R_1]$ and $a = R_2/R_1$ and $\gamma = \sigma_2/\sigma_1$.

We now define an initial condition for the formulation of the temporal linear stability analysis. We assume that at $t = 0$, the cylindrical interfacial geometry of the base state is perturbed by an axisymmetric disturbance with scale $\delta(\ll 1)$. We use a cylindrical coordinate system (r, θ, z) where the z-axis coincides with the core axis in the base state. For axisymmetric disturbances at the inner and/or outer interfaces, the interfacial locus is specified non-dimensionally as $r = f_1(z, t)$ and $r = f_2(z, t)$, (lengths are scaled with R_1 and time by $[(\rho_1 R_1^3)/\sigma_1]^{1/2}$ and the initial condition is specified as

$$f_1(z, t = 0) = 1 + \zeta_{1,0}^{[1]}(z)\delta \quad \text{and} \quad f_2(z, t = 0) = a + \zeta_{2,0}^{[1]}(z)\delta$$

where the superscript [1] denotes the order of the expansion in δ. The initial velocities in the core and the annular region are assumed to be zero. The initial interfacial disturbances cause hydrodynamic flow and interfacial motion for $t > 0$. Since the fluid is assumed incompressible and the motion is axisymmetric, the non-dimensional components of velocity (u_i and w_i in the r- and z-directions, respectively), can be described in terms of a (non-dimensional) stream function $\Psi_i(r, z)$:

$$u_i = \frac{1}{r}\frac{\partial \Psi_i}{\partial z}, \quad w_i = -\frac{1}{r}\frac{\partial \Psi_i}{\partial r}. \tag{2}$$

Here, velocities are scaled as $(\sigma_1/(\rho_1 R_1))^{1/2}$ and the stream function by $R_1^2(\sigma_1/(\rho_1 R_1))^{1/2}$. The stream function, interfacial deflections and pressure can be expanded in δ:

$$f_1(z, t) = 1 + \zeta_1^{[1]}(z, t)\delta + O(\delta^2), \tag{3}$$

https://doi.org/10.1017/S0022112000001282 Published online by Cambridge University Press

$$f_2(z,t) = a + \zeta_2^{[1]}(z,t)\delta + O(\delta^2), \tag{4}$$

$$[\Psi_i(r,z,t), p_i(r,z,t)] = [\Psi_i^{[1]}(r,z,t)\delta,\ p_i^{[0]} + p_i^{[1]}(r,z,t)\delta] + O(\delta^2), \tag{5}$$

where $\zeta_i^{[1]}(z,t=0) = \zeta_{i,0}^{[1]}(z)$, and the evolution in time of the first-order quantities define the linear stability.

Substituting the expansion for the stream function into the Navier–Stokes equation for the stream function and retaining the terms first order in δ, results in a linear differential equation for $\Psi_i^{[1]}(r,z,t)$. Fourier transforming in z (wavenumber k) and Laplace transforming in time (parameter s) yields the following equation in r:

$$\mathrm{D}\left(\mathrm{D} - \frac{\boldsymbol{J}^{1/2} d_i s}{m_i}\right)\Psi_i(r,k,s) = 0, \tag{6}$$

$$\mathrm{D} = \frac{\mathrm{d}^2}{\mathrm{d}r^2} - \frac{1}{r}\frac{\mathrm{d}}{\mathrm{d}r} - k^2$$

The dimensionless parameters introduced in (6) are: $\boldsymbol{J} = \rho_1\sigma_1 R_1/\mu_1^2$, $m_1 = 1$, $m_2 = m = \mu_2/\mu_1$, $d_2 = d = \rho_2/\rho_1$ and $d_1 = 1$. The variable $\Psi_i(r,k,s)$ (without the superscript) denotes the Fourier–Laplace transform of the first-order stream function. The transforms of the first-order stream function and the interfacial deformations (to be used in the boundary conditions below) are defined as

$$\begin{bmatrix} \Psi_i(r,k,s) \\ \zeta_i(k,s) \end{bmatrix} = \int_{-\infty}^{\infty}\left[\int_0^{\infty}\begin{bmatrix} \Psi_i^{[1]}(r,z,t) \\ \zeta_i^{[1]}(z,t) \end{bmatrix} \mathrm{e}^{-st}\,\mathrm{d}t\right] \mathrm{e}^{-\mathrm{i}kz}\,\mathrm{d}k. \tag{7}$$

The linearized first order in δ boundary conditions in dimensionless form in the Fourier–Laplace domain are:

(a) at $r = 0$, the velocity is bounded:

$$\Psi_1 < \infty, \tag{8}$$

$$\frac{\mathrm{d}\Psi_1}{\mathrm{d}r} < \infty; \tag{9}$$

(b) at $r = 1$, the velocity is continuous, the tangential stresses on either side balance, the normal stresses balance the capillary force and the kinematic condition relates the interfacial deflection to the radial velocity:

$$\Psi_1 = \Psi_2, \tag{10}$$

$$\frac{\mathrm{d}\Psi_1}{\mathrm{d}r} = \frac{\mathrm{d}\Psi_2}{\mathrm{d}r}, \tag{11}$$

$$m[\mathrm{D}\Psi_2 + 2k^2\Psi_2] = [\mathrm{D}\Psi_1 + 2k^2\Psi_1], \tag{12}$$

$$\frac{m}{\mathrm{i}kr}\frac{\mathrm{d}}{\mathrm{d}r}\left[\left(\mathrm{D} - s\boldsymbol{J}^{1/2}\frac{d}{m}\right)\Psi_2\right] + 2mik\frac{\mathrm{d}}{\mathrm{d}r}\left[\frac{1}{r}\Psi_2\right]$$
$$-\frac{1}{\mathrm{i}kr}\frac{\mathrm{d}}{\mathrm{d}r}[(\mathrm{D} - s\boldsymbol{J}^{1/2})\Psi_1] - 2\mathrm{i}k\frac{\mathrm{d}}{\mathrm{d}r}\left[\frac{1}{r}\Psi_1\right] = \boldsymbol{J}^{1/2}[k^2 - 1]\zeta_1, \tag{13}$$

$$\zeta_1 = \frac{\mathrm{i}k\Psi_1}{s} + \frac{\zeta_{1,0}}{s}; \tag{14}$$

(c) at $r = a$, the tangential stress is equal to zero, the normal stress balances the

https://doi.org/10.1017/S0022112000001282 Published online by Cambridge University Press

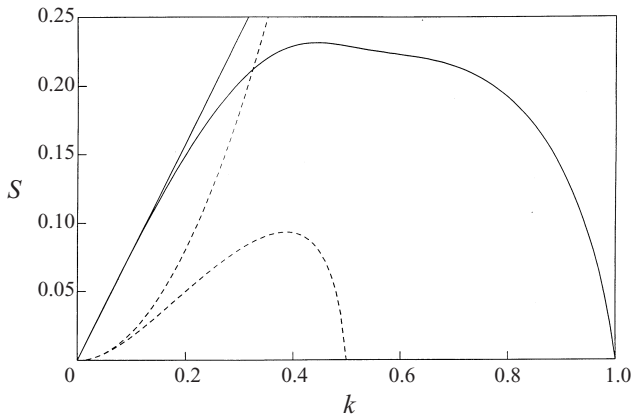


FIGURE 3. The two growing temporal modes (the curves that intersect the k-axis twice) and their long-wavelength limits. $a = 2$, $d = 1$, $\gamma = 2$, $m = 1$, $\boldsymbol{J} = 1000$. ———, Stretching; - - - - -, squeezing.

capillary force and the kinematic condition relates the interfacial deflection of the outer interface to its radial velocity:

$$\mathrm{D}\Psi_2 + 2k^2\Psi_2 = 0, \tag{15}$$

$$\frac{m}{\mathrm{i}kr}\frac{\mathrm{d}}{\mathrm{d}r}\left[\left(\mathrm{D} - s\boldsymbol{J}^{1/2}\frac{d}{m}\right)\Psi_2\right] + 2mik\frac{\mathrm{d}}{\mathrm{d}r}\left[\frac{1}{r}\Psi_2\right] = -\gamma\boldsymbol{J}^{1/2}\left[k^2 - \frac{1}{a^2}\right]\zeta_2, \tag{16}$$

$$\zeta_2 = \frac{\mathrm{i}k\Psi_2}{as} + \frac{\zeta_{2,0}}{s}; \tag{17}$$

$\zeta_{l,0}$ denotes the Fourier transform of the initial deflections $\zeta_{i,0}^{[1]}(z)$. Solution of (6) yields

$$\Psi_i(r) = A_i rI_1(kr) + B_i rK_1(kr) + D_i rI_1(\beta_i r) + E_i rK_1(\beta_i r), \tag{18}$$

where I_1 and K_1 are the modified Bessel function of order 1, and A_i, B_i, D_i, E_i are the constants of integration, which can depend on the wavenumber k and $\beta_i^2 = k^2 + s\boldsymbol{J}^{1/2}d_i/m_i$ for $i = 1, 2$. Substituting (18) into the boundary conditions leads to the implicit matrix equation $\boldsymbol{A}(s,k)\boldsymbol{x} = \boldsymbol{b}$ for the growth rate $s(k)$. $\boldsymbol{A}(s,k)$ is a 8×8 matrix (see Appendix) and

$$\boldsymbol{b}^t = [0, 0, 0, 0, 0, 0, \mathrm{i}\zeta_{1,0}, \mathrm{i}\zeta_{2,0}], \tag{19}$$

$$\boldsymbol{x}^t = [A_2, B_2, D_2, E_2, A_1, D_1, -\mathrm{i}\zeta_1, -\mathrm{i}\zeta_2]. \tag{20}$$

If $\boldsymbol{A}$ is non-singular, $\boldsymbol{x}(k,s) = \boldsymbol{A}^{-1}(k,s)\boldsymbol{b}(k)$. This, in combination with (18), gives the solution in the Fourier–Laplace domain. Its inversion into the space–time domain is performed in the Appendix.

The growth rates $s_n(k)$ (n denoting the mode) are the zeros of the implicit dispersion equation $\det(\boldsymbol{A}(k,s)) = 0$. Since the dispersion equation is transcendental, there may be an infinite number of roots for a given k; we examine only the unstable roots, because the stable roots decay and do not contribute at long times. Long-wave results (see § 3.1) show that there are three system modes whose growth rates go to zero as $k \to 0$. These represent three modes of the system. There are other solutions of the dispersion equation but they are all stable. Two of the three modes whose growth rates go to zero as $k \to 0$ are unstable, i.e. the real part of the growth rate is positive, and the third is stable. The growth rate of the two growing modes as a function of the wavenumber is shown in figure 3; these two modes are identical to the ones identified

https://doi.org/10.1017/S0022112000001282 Published online by Cambridge University Press

in the previous studies mentioned above: the growth rate of the first mode is real and positive for $k < 1$, i.e. this mode is unstable to all waves with wavelength greater than the undisturbed core circumference. The second mode has a real and positive growth rate for $k < 1/a$, implying that it is unstable to all disturbances with wavelength greater than the undisturbed outer circumference of the annulus. After calculating the growth rate and substituting into the dispersion equation, one finds the amplitude ratio in the Fourier–Laplace domain, i.e. ζ_2/ζ_1. The growing mode whose growth rate goes to zero at $k = 1/a$ has a real and negative amplitude ratio for $0 < k < 1/a$. This implies that the two interfaces grow out of phase and thus squeeze the film fluid; hence the name squeezing mode. The other growing mode, whose growth rate goes to zero at $k = 1$, has a real and positive amplitude ratio for $0 < k < 1$. This implies that the two interfaces grow in phase, i.e. the film stretches; hence, the stretching mode. Figure 2 shows the stretching and squeezing modes. At $k = 1/a$, the circumferential curvature of the outer interface balances the longitudinal curvature. Since the growth rate of the squeezing mode goes to zero at $k = 1/a$, it is necessary that the forces due to surface tension balance on the inner surface as well. The only way that this is possible, if $k \neq 1$, is if $\zeta_1 = 0$. So, $\zeta_2/\zeta_1 = \infty$. Similarly, for the stretching mode at $k = 1$, $\zeta_2/\zeta_1 = 0$.

3. Asymptotic results

3.1. *Long waves* ($k \to 0$)

In the limit $k \to 0$, since the wavenumber is non-dimensionalized by R_1, waves are longer than the outer circumference, so both the squeezing and stretching modes are unstable. This long-wave limit implies that the length scales in the axial direction are much longer than the length scales in the radial direction, for both the core and the annulus. Regular expansions in k of the stream functions and the growth rate s can be inserted into the linear stability equations to determine analytically the coefficients of these expansions. The validity of assuming regular expansions is verified by a direct expansion of the elements of the coefficient matrix $\boldsymbol{A}(s,k)$ as we explain below.

Assuming regular expansions of s and Ψ_i in k, i.e.

$$s = s^{(1)}k + s^{(2)}k^2 + O(k^3), \tag{21}$$

$$\Psi_i = \Psi_i^{(0)} + \Psi_i^{(1)}k + \Psi_i^{(2)}k^2 + O(k^3), \tag{22}$$

substituting these into the governing equation and boundary conditions, and solving the leading-order problem in k, yields the following solutions to the growth rate:

(i) stretching mode

$$s = \pm\sqrt{\frac{1+a\gamma}{2(a^2d-d+1)}}k + O(k^2), \tag{23}$$

$$\frac{\zeta_2}{\zeta_1} = a + O(k);$$

(ii) squeezing mode

$$s = \frac{\gamma \boldsymbol{J}^{1/2}}{16ma^3(1+\gamma a)}(4a^4\ln(a) + (m-3)a^4 + 2(2-m)a^2 + m - 1)k^2 + O(k^3), \tag{24}$$

$$\frac{\zeta_2}{\zeta_1} = -\frac{1}{\gamma} + O(k).$$

https://doi.org/10.1017/S0022112000001282 Published online by Cambridge University Press

The asymptotic limits ($k \to 0$) of the two growing modes are compared with the numerical solutions in figure 3, and the agreement is excellent for long waves, validating the numerics.

Another way of getting these asymptotic results is by separating the modified Bessel functions K_0 into their logarithmic and the algebraic parts: $K_n(z) = g_n(z) + (-1)^{n+1} \ln(z/2) I_n(z)$, where $g(z)$ is real. By multiplying Column 1 of the matrix $\boldsymbol{A}$ by $\ln(ka/2)$ and subtracting it from Column 2 one can eliminate the $\ln(k)$ terms in the expansion of K_n. Similarly, by multiplying Column 3 by $\ln(\beta_2 a)$ and subtracting from Column 4, one can eliminate the remaining $\ln(k)$ terms in the determinant. Thus, it is consistent to assume, as above, regular expansions of Ψ_i and s in k. If one expands the remaining terms in the determinant in k (using the symbolic algebraic operations in *Mathematica* for instance), the determinant gives the same roots as obtained above.

The simplification of the continuity and equations of motion in the long-wavelength limit allow a clear interpretation of the dynamics of both modes, including how the amplitude ratio is fixed, and insight into the dependence of the leading-order growth rate on the tension, density and viscosity ratios as given by (23) and (24). As $k \to 0$, the circumferential curvature $-\zeta_2^{[0]}/a^2$ at $r = a$ creates in the underlying annular liquid a zeroth-order stress normal to the surface, $[p_2^{[0]} - \tau_{2[rr]}^{[0]}]_{r=1+a}$, equal to $-\gamma\zeta_2^{[0]}/a^2$. In this notation of the primitive variables for the perturbed quantities (all in non-dimensional form and in the Fourier–Laplace domain), the superscript is the order in k, $\tau_{2[rr]}^{[0]}$ is the viscous stress ($= 2(m/\sqrt{\boldsymbol{J}})(\mathrm{d}u_2^{[0]}/\mathrm{d}r)$) and is scaled with σ_1/R_1. From the formal development above or the reasoning which will be evident below, the leading-order growth rate and radial velocity are of order k (stretching mode) or k^2 (squeezing mode). Thus $\tau_{2[rr]}^{[0]}$ is equal to zero and there is no radial acceleration at leading order; the r component of the equation of motion at $O(k^0)$ is

$$\frac{\mathrm{d}p_2^{[0]}}{\mathrm{d}r} = 0, \tag{25}$$

and the leading-order pressure is in fact constant with the constant imposed by the normal stress condition at the outer interface:

$$p_2^{[0]}(r) = -\gamma\zeta_2^{[0]}/a^2, \tag{26}$$

Similarly for the core phase $0 = -(\mathrm{d}/\mathrm{d}r)\{p_1^{[0]}\}$, and the constant core pressure can be related to the deformation at the core/annular fluid interface $r = 1$ by the normal stress balance there:

$$p_1^{[0]}(r) = -[\gamma\zeta_2^{[0]}/a^2 + \zeta_1^{[0]}]. \tag{27}$$

The zeroth-order pressures create order-k axial pressure gradients which drive in both phases a first-order viscous stress ($\tau_{i[rz]}^{[1]}$) and axially accelerate the fluid ($d_i s^{[1]} w_i^{[0]}$) as described by the order-k axial equation of motion:

$$d_i s^{[1]} w_i^{[0]} = -\mathrm{i}p_i^{[0]} + \frac{1}{r}\frac{\mathrm{d}}{\mathrm{d}r}[r\tau_{i[rz]}^{[1]}], \tag{28}$$

where $w_i^{[j]}(r)$ is the axial velocity of order j and $\tau_{i[rz]}^{[1]} = (m_i/\sqrt{\boldsymbol{J}})(\mathrm{d}w_i^{[1]}/\mathrm{d}r)$. The zeroth-order axial velocity $w_i^{[0]}(r)$ which appears in the axial acceleration in (28) is independent of r, as can be deduced from the zeroth-order axial equation of motion:

$$0 = \frac{1}{r}\frac{\mathrm{d}}{\mathrm{d}r}[r\tau_{i[rz]}^{[0]}], \tag{29}$$

where $\tau_{i[rz]}^{[0]} = (m_i/\sqrt{\boldsymbol{J}})(\mathrm{d}w_i^{[0]}/\mathrm{d}r)$ is the zeroth-order shear stress. The zeroth-order

https://doi.org/10.1017/S0022112000001282 Published online by Cambridge University Press

axial inertia in (29), $d_i s^{[0]} w_i^{[0]}$, is equal to zero since s leads with k or k^2. Thus the zeroth-order shear stress is a constant divided by r in each phase. Since the gas exerts no shear on the outer surface, and the zeroth-order stresses are continuous at $r = 1$, $\tau_{i[rz]}^{[0]}$ is zero and the zeroth-order axial velocities in each phase are constant and (by continuity of velocity at $r = 1$) equal to each other. The zeroth-order axial velocity ($w_i^{[0]}$) has a first-order radial flow $u_i^{[1]}(r)$ linear in r obtained by the equation of continuity:

$$\left.\begin{aligned} u_1^{[1]}(r) &= -\mathrm{i}\tfrac{w^{[0]}}{2} r \quad (0 < r < 1) \\ u_2^{[1]}(r) &= -\mathrm{i}\tfrac{w^{[0]}}{2} r \quad (1 < r < a) \end{aligned}\right\} \tag{30}$$

From the kinematic conditions $s^{[1]}\zeta_2^{[0]} = -\mathrm{i}\frac{1}{2} w^{[0]} a$ and $s^{[1]}\zeta_1^{[0]} = -\mathrm{i}\frac{1}{2} w^{[0]}$ and therefore

$$\frac{\zeta_2^{[0]}}{\zeta_1^{[0]}} = a \quad \text{for} \quad w^{[0]} \neq 0. \tag{31}$$

The long-wave dynamics of the two unstable modes are different, and the origin of this difference is the presence of the zeroth-order axial velocity. In the stretching mode, $\zeta_2^{[0]}/\zeta_1^{[0]} > 0$; thus from (31) the amplitude ratio is equal to a and $p_1^{[0]}(r) = -[(\gamma/a + 1)\zeta_1^{[0]}]$. In (28), the axial velocity can be replaced by the interfacial deflection using the kinematic condition, and pressures can be replaced by their relations to the interfacial deflections to obtain an equation in $\zeta_2^{[0]}$. By multiplying this relation by r and integrating in r from 0 to 1 for region 1 and from 1 to a for region 2, and adding, one arrives at a solvability equation for $s^{[1]}$. Since the first-order shear stress is zero at $r = a$, and continuous at $r = 1$, this solvability condition is independent of the first-order shear stress, and becomes identical to (23). Thus in the long-wave dynamics for the stretching mode, the circumferential-driven axial pressure gradient accelerates the fluid in both regions, and the growth rate is a function of the core and annular densities. Because the first-order stress is zero at the outer interface, the integrability condition explains why the growth rate is independent of the fluid viscosities (cf. (23)). The stretching flow itself to leading order is locally a bi-axial extension, with the axial flow of order-k^0 and independent of radial position and the radial flow of order-k and linear in r, and the amplitude ratio fixed at a by the kinematic conditions.

In the squeezing mode, $\zeta_2^{[0]}/\zeta_1^{[0]} < 0$, and therefore $w^{[0]}$ is equal to zero from (31). The axial velocity in this mode consequently leads with k, and by continuity and the kinematic condition, the radial velocity and the growth rate lead with k^2. The axial equation of motion contains no inertia to order-k, and the axial pressure gradients drive only viscous flow as detailed by (28). Integrating (28) as before yields

$$\mathrm{i}\frac{\gamma\zeta_2^{[0]}}{2}\left[1 - \frac{1}{a^2}\right] = \tau_{2[rz]}^{[1]}, \quad \mathrm{i}\frac{1}{2}\left[\zeta_1^{[0]} + \gamma\frac{\zeta_2^{[0]}}{a^2}\right] = -\tau_{1[rz]}^{[1]} \quad (r = 1), \tag{32}$$

where we have used the fact that the first-order shear stress is zero at $r = a$. Since the shear stress is continuous at $r = 1$, addition of the above gives the amplitude ratio $\zeta_2^{[0]}/\zeta_1^{[0]} = -1/\gamma$. The axial pressure gradient in the annular region applies a first-order shear stress to the core equal to $\mathrm{i}\frac{1}{2}\gamma\zeta_2^{[0]}[1 - 1/a^2]$, and the amplitude of the inner surface adjusts so that the pressure gradient in the core balances the applied shear stress. It is this balancing of forces which determines the amplitude ratio in the squeezing mode, rather than the kinematic constraint as in the stretching mode. Integrating (28) in each region, and using the continuity of axial velocity and shear

https://doi.org/10.1017/S0022112000001282 Published online by Cambridge University Press

stress at $r = 1$, the kinematic conditions and the fact that the first-order shear stress is equal to zero at $r = a$, results in the dispersion equation (24). Since there is no inertia, the growth rate is independent of the fluid densities. Note in (24) the density ratio d does not appear; the factor of $\boldsymbol{J}^{1/2}$ which contains the density of the core fluid emerges from the relation for the first-order shear stress in terms of the velocity gradient due to the non-dimensionalization of velocity using ρ_1. (The dimensional growth rate multiplies equation (24) by $(\sigma_1/(\rho_1 R_1^3))^{1/2}$ and the dependence on the core density is removed.)

3.2. *Thin films* ($a \to 1$)

If the film is thin with respect to the undisturbed core radius R_1, it is convenient to define a parameter $\epsilon = (R_2 - R_1)/R_1 = a - 1$, the dimensionless film thickness, which is small compared with one. The dimensionless radial length scale in the film is $O(\epsilon)$ while the film's dimensionless axial scale and all dimensionless core length scales remain $O(1)$. As a result, the radial derivatives in the film are relatively large, i.e. $O(1/\epsilon)$. In order to rescale the rapid radial variation in the film we stretch the radial length scale via the change of variables $y \equiv (r-1)/\epsilon$, where y-derivatives in the annulus are $O(1)$. One can expand the solutions in powers of ϵ and match core and annulus solutions in orders of ϵ.

To determine which scalings of s in ϵ will be appropriate, one can guess that these scales persist even in the long-wave regime. Then, one expands the three long-wave asymptotic results in powers of ϵ to extract these scales analytically. For the three modes, respectively, one gets

$$s = \pm\sqrt{\frac{1+\gamma}{2}}\epsilon^0 k + O(\epsilon), \tag{33}$$

$$s = \frac{\boldsymbol{J}^{1/2}\gamma}{4(1+\gamma)}\epsilon^2 k^2 + O(\epsilon^3). \tag{34}$$

Two of the roots scale as ϵ^0 and one root scales as ϵ^2. For each mode, we then substitute regular expansions for s and Ψ_i into the differential equation and the boundary conditions and solve the leading-order problem in ϵ.

As a means of checking our results we expand these expressions for s in the long-wave limit of $k \to 0$. These results are identical to (33) and (34), i.e. those obtained by taking the limit $\epsilon \to 0$ of the long-wave results.

(i) Stretching mode

For the ϵ^0 mode, assume the regular expansions of s and Ψ_i in ϵ,

$$s = s^{[0]} + s^{[1]}\epsilon + s^{[2]}\epsilon^2 + O(\epsilon^3), \quad \Psi_i = \Psi_i^{[0]} + \Psi_i^{[1]}\epsilon + \Psi_i^{[0]}\epsilon^2 + O(\epsilon^3). \tag{35}$$

The leading-order problem gives an implicit equation for $s^{[0]}$. The solution is

$$\begin{aligned}(k^2-1)k(1+\gamma)I_1(k)I_1(\beta) - 4k^3\beta I_1(k)\left(I_0(\beta) - \frac{I_1(\beta)}{\beta}\right) \\ + 2k^2\left(I_0(k) - \frac{I_1(k)}{k}\right)(s^{[0]} + 2k^2)I_1(\beta) \\ + \boldsymbol{J}^{1/2}s^{[0]}I_0(k)I_1(\beta)(\boldsymbol{J}^{1/2}s^{[0]} + 2k^2) = 0,\end{aligned} \tag{36}$$

where

$$\beta = \sqrt{k^2 + \boldsymbol{J}^{1/2}s^{[0]}}. \tag{37}$$

https://doi.org/10.1017/S0022112000001282 Published online by Cambridge University Press

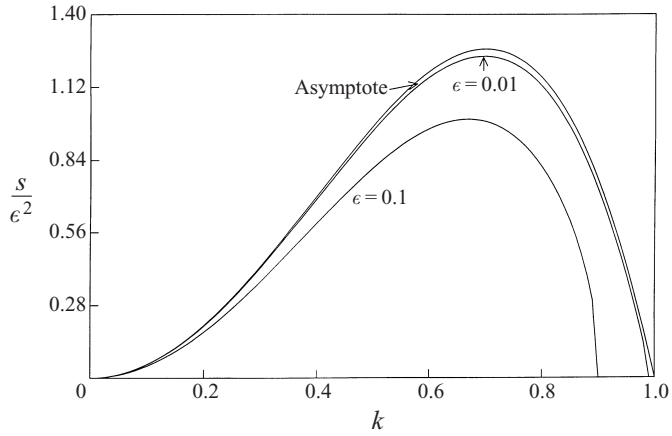


FIGURE 4. Thin-film ($\epsilon \to 0$) limit for the squeezing mode. $d = 1$, $\gamma = 2$, $m = 1$, $\boldsymbol{J} = 1000$.

We recognize that the dispersion equation (36) is identical to that for a single jet with $\sigma = \sigma_1 + \sigma_2$. The amplitude ratio is given as

$$\frac{\zeta_2}{\zeta_1} = 1 + O(\epsilon). \tag{38}$$

(ii) Squeezing mode

For the ϵ^2 mode, assume the regular expansions

$$s = s^{[2]}\epsilon^2 + O(\epsilon^3), \tag{39}$$

$$\Psi_i = \Psi_i^{[0]} + \Psi_i^{[1]}\epsilon + O(\epsilon^2). \tag{40}$$

In this case one can solve for the leading order growth rate $s^{[2]}$ explicitly:

$$s^{[2]} = \boldsymbol{J}^{1/2} k \frac{(1-k^2)}{2I_1(k)} F_1(k) \frac{\gamma}{1+\gamma}, \tag{41}$$

where

$$F_1(k) = -k\frac{I_0^2(k)}{I_1(k)} + kI_1(k) + 2I_0(k). \tag{42}$$

The amplitude ratio is given by

$$\frac{\zeta_2}{\zeta_1} = -\frac{1}{\gamma} + O(\epsilon). \tag{43}$$

In figures 4 (for the squeezing mode) and 5 (for the stretching mode) we compare the leading-order asymptotic expressions with exact numerical solutions, and we note that the asymptotes merge with the numerical solutions for ϵ smaller than 0.01.

In the thin-film limit (like the long-wave limit), the rescaling of the equations of continuity and motion in the annular region provide simplified expressions which make the dynamics apparent. Again the deflection of the outer surface creates a zero-order normal stress in the annular liquid underneath the surface. Because wavenumbers are of order one in ϵ, the capillary force contains both the circumferential destabilization and the stabilizing axial curvature, i.e. $[p_2^{[0]} - \tau_{2[rr]}^{[0]}]_{y=1}$, equal to $\gamma\zeta_2^{[0]}(k^2-1)$. In this primitive variables notation, the superscript is the order in ϵ, $\tau_{2[rr]}^{[0]}$ is the viscous stress ($= 2(m/\sqrt{\boldsymbol{J}})(\mathrm{d}u_2^{[1]}/\mathrm{d}y)$) and is scaled with σ_1/R_1. The rescaling of the equation of

https://doi.org/10.1017/S0022112000001282 Published online by Cambridge University Press

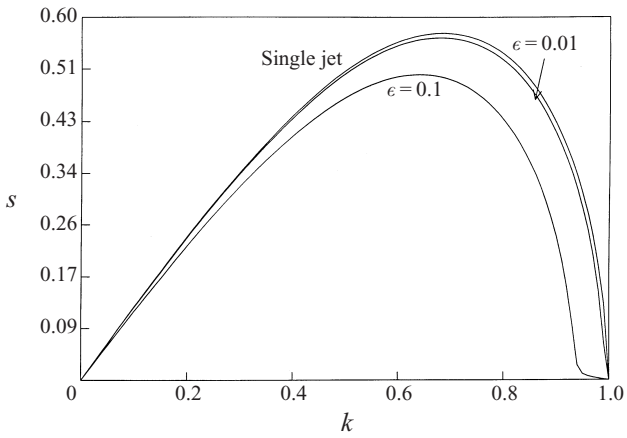


FIGURE 5. Thin-film ($\epsilon \to 0$) limit for the stretching mode. $d = 1$, $\gamma = 2$, $m = 1$, $\boldsymbol{J} = 1000$.

motion in the r-direction shows that this normal stress does not depend on y, even if there exists a zeroth-order radial acceleration:

$$0 = -\frac{\mathrm{d}}{\mathrm{d}y}\{p_2^{[0]} - \tau_{2[rr]}^{[0]}\}, \quad p_2^{[0]} - \tau_{2[rr]}^{[0]} = \gamma\zeta_2^{[0]}(k^2 - 1). \tag{44}$$

The order-zero pressure in the film drives an axial viscous flow with order-one shear stress ($\tau_{2[yz]}^{[1]}$) and a zeroth-order acceleration of the film fluid ($ds^{[0]}w_2^{[0]}$) as described by the order-ϵ^0 axial equation of motion:

$$ds^{[0]}w_2^{[0]} = -\mathrm{i}k[p_2^{[0]} - \tau_{2[zz]}^{[0]}] + \frac{\mathrm{d}}{\mathrm{d}y}[\tau_{2[rz]}^{[1]}]. \tag{45}$$

The zero-order shear stress $\tau_{2[rz]}^{[0]}$ in the film does not vary with y because the pressure gradient is of order zero, thus

$$0 = \frac{\mathrm{d}}{\mathrm{d}y}[\tau_{2[rz]}^{[0]}]. \tag{46}$$

Since the zero-order stress is zero at the outer interface, $[\tau_{2[rz]}^{[0]}]$ is everywhere zero in the film. The zero-order axial flow $w_2^{[0]}$ is uniform in y, as follows from the ϵ^{-2} axial equation of motion.

In the stretching mode, $\zeta_2^{[0]}/\zeta_1^{[0]} > 0$. The normal stress balance at the core/film interface to leading order becomes

$$[p_1^{[0]} - \tau_{1[rr]}^{[0]}]_{r=1} = -[\zeta_1^{[0]}(1 - k^2) + \gamma\zeta_2^{[0]}(1 - k^2)]. \tag{47}$$

Since in the ST mode, $\zeta_2^{[0]}/\zeta_1^{[0]} > 0$, the capillary pressures drive an order-ϵ^0 flow in the core ($w_1^{[0]}$ and $u_1^{[0]}$), which can be described by a zero-order stream function $\Psi_1^{[0]}(r, z)$ satisfying equation (6). At the core/film interface we have already noted that $[\tau_{2[rz]}^{[0]}]$ is everywhere zero in the film, so by continuity $[\tau_{1[rz]}^{[0]}(r = 1)]$ is zero, i.e. the film cannot support a zero-order shear stress generated by the capillary forces in the core. Also at the interface, the zero-order flow in the core entrains, by continuity, zero-order flows $w_2^{[0]}$ and $u_2^{[0]}$ in the film. We have already remarked that a zero-order axial flow in the film, $w_2^{[0]}$, should be independent of y. By the equation of continuity, the radial flow is also independent of y. Since the radial velocities of the two interfaces are equal, it follows from the kinematic conditions that $\zeta_1^{[0]} = \zeta_2^{[0]}$, and the amplitude ratio for the

https://doi.org/10.1017/S0022112000001282 Published online by Cambridge University Press

stretching mode in this limit is equal to one. (We note that the kinematic constraint also fixes the ST mode amplitude ratio for $k \to 0$ as $1/a$: in the common limit $k \to 0$ and $\epsilon \to 0$ both the k and ϵ expansions for the amplitude ratio agree.) With the amplitude ratio equal to one, the normal stress balance becomes

$$[p_1^{[0]} - \tau_{1[rr]}^{[0]}]_{r=1} = -(1+\gamma)[\zeta_1^{[0]}(1-k^2)]. \tag{48}$$

This condition, together with the fact that the zero-order shear stress is zero at the core/film interface closes the core problem, and we see as shown formally above that in the thin-film limit, $s^{[0]}$ for the ST mode is that of a single jet of radius R_1 and tension $\sigma_1 + \sigma_2$ (see figure 5). The stretching flow in the film is zero order in ϵ, as $\epsilon \to 0$, with radial and axial velocities independent of y.

For the SQ mode, the zero-order pressure in the core must be equal to zero. Otherwise, as in the ST mode, this gradient will drive a zeroth-order flow in the core, which induces a zeroth-order flow in the film. As we showed above, the radial velocity in this zeroth-order film flow is independent of y by continuity, and thus, by the kinematic condition, fixes the amplitude ratio at one. For squeezing motion, the amplitude ratio must be negative. From (47) we note that if, to leading order, the deflection of the inner interface $\zeta_1^{[0]} = -\gamma\zeta_2^{[0]}$, then the normal stress in the core underneath the interface $[p_1^{[0]} - \tau_{1[rr]}^{[0]}]_{r=1}$ is zero, and capillary forces do not drive a zero-order flow. Thus the amplitude ratio in the squeezing mode is equal to $-1/\gamma$. In the film we noted above that the zero-order pressure drives a first-order shear stress ($\tau_{2[rz]}^{[1]}$) which when applied to the core creates a first-order flow field there. The velocities associated with this flow are $w_1^{[1]}$ and $u_1^{[1]}$. In principle, they induce first-order velocities in the film. The first-order axial velocity in the film is a constant in y because the zero-order shear stress in the film, $\tau_{2[rz]}^{[0]}$, as we showed above, is zero and $\tau_{2[rz]}^{[0]} = (m/\sqrt{\boldsymbol{J}})(\mathrm{d}w_2^{[1]}/\mathrm{d}y)$. The first-order radial flow in the film must be zero; by continuity $u_2^{[1]}$ is independent of y and therefore the amplitude ratio would be positive, which is not allowed for this mode. Thus we require in particular that the first-order radial velocity equal zero at the core/film interface. However, the first-order axial flow, by continuity, creates a second-order radial flow $u_2^{[2]}$ which is linear in y, since $w_2^{[1]}$ is independent of y. Thus to leading order, the stretching flow in the film consists of a first-order axial velocity and a derived second-order radial velocity which is linear in y to describe the change in sign of the radial velocity across the film in the SQ mode. The second-order radial velocity and the kinematic condition require that the growth rate lead with ϵ^2. If the continuity equation is integrated over the film, the difference in radial velocities at the two interfaces is proportional to the axial velocity,

$$u_2^{[2]}(y=1) - u_2^{[2]}(y=0) = -\mathrm{i}kw_2^{[1]}. \tag{49}$$

It follows from the kinematic conditions and the amplitude ratio that the growth rate is proportional to the axial velocity, and inversely proportional to $1+\gamma$:

$$s^{[2]}\zeta_2^{[0]} = -\frac{\mathrm{i}kw_2^{[1]}}{1+\gamma}. \tag{50}$$

The axial velocity in the film at order one can be obtained from closure of the core problem: The order-one radial velocity in the core is required to be zero at the core/film interface. Furthermore, the first-order traction which drives the first-order flow in the core can be obtained by integrating (45) noting that fluid acceleration and

https://doi.org/10.1017/S0022112000001282 Published online by Cambridge University Press

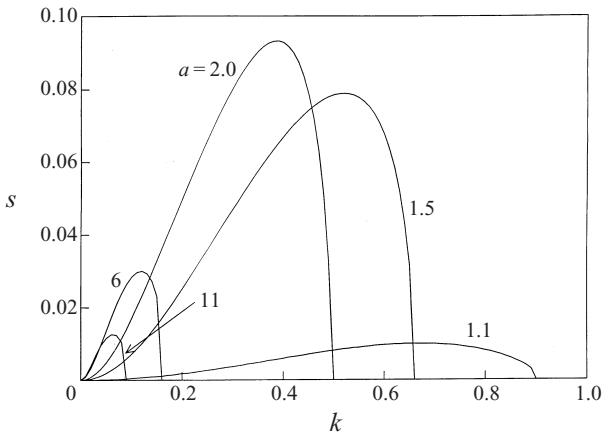


FIGURE 6. $a \to \infty$ limit for the squeezing mode. $d = 1$, $\gamma = 2$, $m = 1$, $\boldsymbol{J} = 1000$.

zero-order stress are zero:

$$\tau^{[1]}_{2[rz]}(y = 0) = \mathrm{i}k\gamma(k^2 - 1)\zeta^{[0]}_2. \tag{51}$$

The shear stress applied to the core is proportional to γ since the capillary pressure of the outer interface is driving this stress. The first-order core velocities (in particular $w^{[1]}_1(r = 1)$) can now be obtained by solving (6) for the stream function in the core. This solution is obtained neglecting the inertial term since s is of order ϵ^2. The conditions on the stream function are that the (first order) radial velocity is zero ($u^{[1]}_1(r = 1) = 0$), and the shear stress equals the first-order film stress

$$(\tau^{[1]}_{1[rz]}(r = 1) = \tau^{[1]}_{2[rz]} \quad (y = 0) \quad \text{or} \quad \frac{1}{\sqrt{\boldsymbol{J}}}\left\{\frac{\partial u^{[1]}_1}{\partial z} + \frac{\partial w^{[1]}_1}{\partial r}\right\}_{r=1} = \mathrm{i}k\gamma(k^2 - 1)\zeta^{[0]}_2).$$

Thus $w^{[1]}_1(r = 1)$ will be proportional to $\gamma\sqrt{\boldsymbol{J}}$; substituting into (50) yields $s^{[2]}$ which is identical to (41), and it is clear now why the growth rate as given by (41) is independent of the film density and viscosity (d and m) and proportional to $\gamma\sqrt{\boldsymbol{J}}/(1 + \gamma)$.

3.3. *Thick films* ($a \to \infty$)

Another limiting case of a compound jet is when the radii ratio $a \to \infty$. The result should be a single jet in an infinite medium (Tomotika 1935). We solved the dispersion equation for this case numerically. In this limit, the squeezing mode disappears because it is unstable only for $k < 1/a$ and, as $a \to \infty, k_{cr}(= 1/a) \to 0$ and its maximum growth rate goes to zero as $a \to \infty$ (figure 6). The Tomotika solution matches the stretching mode solution at $a \sim 10$ (figure 7). The growth rate for the stretching mode becomes independent of the surface tension ratio as the outer interface recedes to infinity.

4. Numerical results for annular films with order-one thicknesses

In this section we present numerical solutions for the case in which the dimensionless annular thickness is of order one. Simulations of the wavenumber (k_{max}) at which the growth rate is the largest, and the growth rate (s_{max}) and amplitude ratio (A_{max}) at k_{max}, as a function of the viscosity, surface tension and density ratios are described. A representative value of $a = 2$ is used for the annular thickness and 10^3 for the viscosity

https://doi.org/10.1017/S0022112000001282 Published online by Cambridge University Press

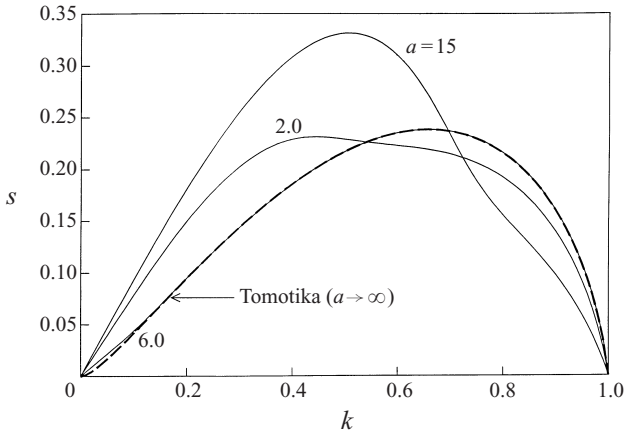


FIGURE 7. $a \to \infty$ limit for the stretching mode. $d = 1$, $\gamma = 2$, $m = 1$, $\boldsymbol{J} = 1000$.

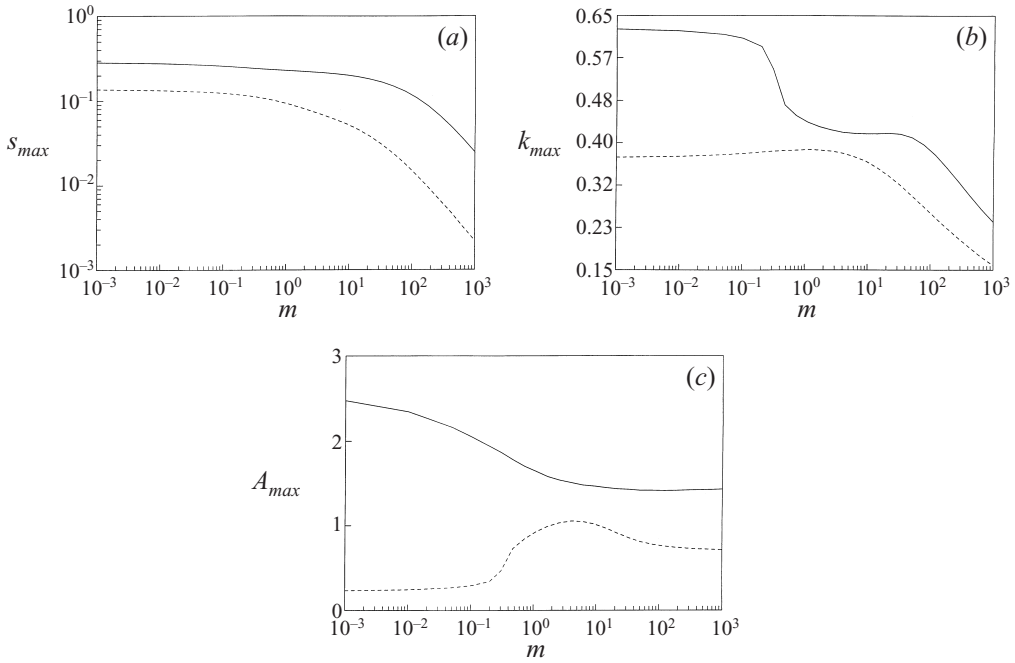


FIGURE 8. Effect of the viscosity ratio m on (*a*) s_{max} (*b*) k_{max}, (*c*) A_{max}. $d = 1$, $a = 2$, $\gamma = 2$, $\boldsymbol{J} = 1000$. ———, Stretching; - - - - -, squeezing.

parameter $\boldsymbol{J}$. Since the growth rate is scaled using core variables (recall time is scaled by $[(\rho_1 R_1^3)/\sigma_1]^{1/2}$ and lengths by R_1) these simulations of the effect of m, γ and d can most easily be interpreted physically as changes in the density and viscosity of the annular layer, and the tension of the outer interface. Thus they address specifically the question of how the properties of the annular layer can be used to adjust the properties of jet breakup.

https://doi.org/10.1017/S0022112000001282 Published online by Cambridge University Press

4.1. *Effect of the viscosity ratio*

Increasing the viscosity of the secondary fluid increases the viscous resistance and thus leads to a decrease in the growth rate (figure 8*a*). The decrease is more pronounced in the squeezing mode because there is more fluid motion due to the squeezing of the annulus. For the entire range of m, the growth rate of the stretching mode is higher. With regard to k_{max}, we note that for the squeezing mode, the maximally growing wavenumber only increases marginally up to approximately 10, and then decreases by approximately one-half for m between 10 and 10^3. For the stretching mode, we find a significant overall reduction of k_{max} with increasing m (figure 8*b*) taken over the entire viscosity range studied ($0.001 < m < 10^3$) and the reduction is from 0.63 to 0.25. However, a plateau region exists for m between 1 and 20. In this range the maximum growth rate also does not change, so we would expect in drop formation applications the breakup length and size to be relatively insensitive to the viscosity ratio for $20 > m > 1$.

An increase in m results in a decrease in both the core and the film velocities. Thus, the amplitude ratio, which is the ratio of the radial velocities at the two interfaces, does not change significantly for both modes (figure 8*c*). In particular for the dominant stretching mode, there is only a change from 2.5 to 1.5.

4.2. *Effect of the surface tension ratio*

The surface tension forces are independent of the film thickness. So the variation in s_{max}, k_{max} and A_{max} with a change in γ for finite film thickness should be qualitatively similar to that in thin films. In the thin-film limit, the growth rate $s(\gamma)$, and hence $s_{max}(\gamma)$, for the squeezing mode is inversely proportional to $1 + 1/\gamma$. We observe the same trend for $\epsilon \sim 1$ as shown in figure 9(*a*). In the thin-film limit, the stretching mode is like a single jet with dimensionless surface tension $1 + \gamma$. A similar trend occurs for finite film thicknesses (figure 9*a*). In the stretching mode, plots (not shown) of the growth rate as a function of the wavenumber indicate that the growth rate increases with an increase in γ for $k < 1/a$ and decreases for $1/a < k < 1$. The reason for this is because an increase in γ results in an increase in the net capillary pressure exerted by the outer interface, which is destabilizing if $k < 1/a$ and stabilizing otherwise. Thus if $k_{max} > 1/a$, s_{max} will decrease with an increase in γ and the reverse will happen if $k_{max} < 1/a$. In figure 9(*b*) the variation in k_{max} with γ is shown. For $\gamma < 1$, $k_{max} > 1/a (= 0.5)$. In this range, s_{max} decreases (figure 9*a*) although the decrease is not evident in the figure. For $\gamma > 1, k_{max} < 1/a$, and s_{max} increases with an increase in γ. The growth rate of the stretching mode is higher than that of the squeezing mode for the entire range of γ; it is again the dominant mode. The variation of k_{max} with γ for the stretching and the squeezing modes as given in figure 9(*b*) indicates a significant decrease in k_{max} with an increase in γ for the stretching mode (0.66 to 0.36) while k_{max} increases, though not as significantly (0.32 to 0.48), with γ for the squeezing mode.

As $\epsilon \to 0$, the amplitude ratio for the stretching and the squeezing modes are 1 and $-1/\gamma$, respectively. When $\epsilon \sim 1$, A_{max} for the squeezing mode follows $-1/\gamma$ closely and A_{max} for the stretching mode is close to 1 (0.8 to 2) for the entire range of γ (figure 9*c*). Thus for the dominant stretching mode, as was the case with the viscosity ratio, the amplitude ratio is not sensitive to the surface tension ratio.

4.3. *Effect of the density ratio*

An increase in the film density increases the core and annular fluid inertias and, since the capillary driving forces do not increase, the growth rate decreases. In the squeezing mode, there is more fluid motion, so its decrease in growth rate is more appreciable,

https://doi.org/10.1017/S0022112000001282 Published online by Cambridge University Press

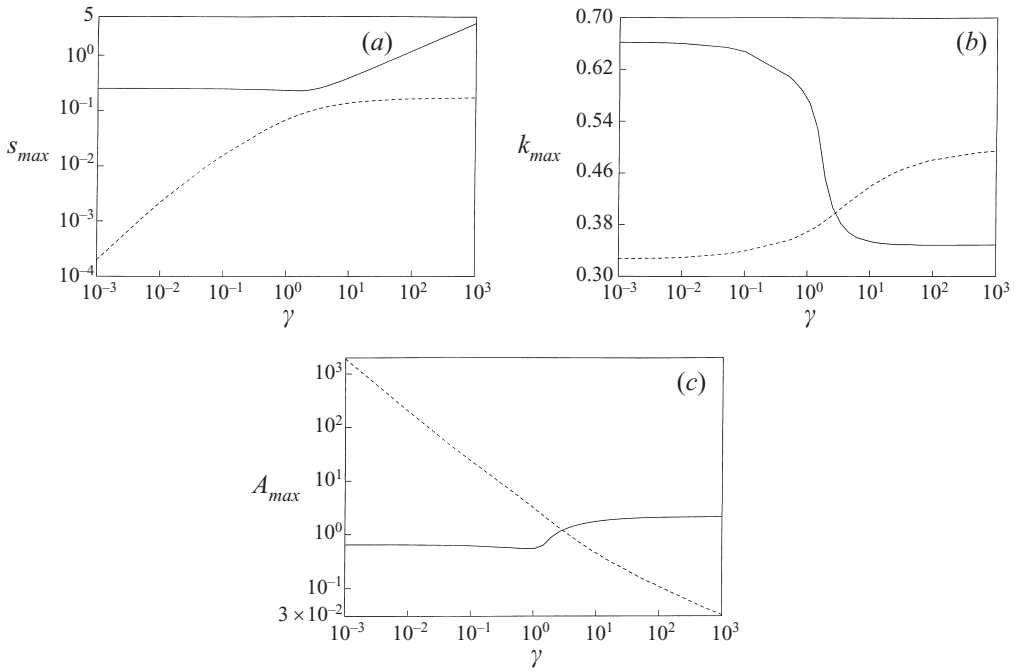


FIGURE 9. Effect of the surface tension ratio γ on (*a*) s_{max} (*b*) k_{max}, (*c*) A_{max}, $d = 1$, $a = 2$, $m = 1$, $\boldsymbol{J} = 1000$. ———, Stretching; - - - - -, squeezing.

but the growth rate of the stretching mode is once again dominant (figure 10*a*). In figure 10(*b*), k_{max} for the squeezing mode decreases slightly with an increase in d while k_{max} for the stretching mode follows an interesting trend: there is a significant increase (0.32 to 0.52) for $d < 1$, a maximum at $k = 1$, and a significant decrease (0.52 to 0.35) for $d > 1$. The amplitude ratio for the stretching mode (figure 10*c*) is sensitive to the density ratio. As d increases from 0.1 to 10, A_{max} decreases from 8 to 0.5, and this order of magnitude change in the ST mode A_{max} is far greater than the variation for the viscosity and surface tension ratios. For the squeezing mode the increase with d is slight (figure 10*c*).

5. Comparison with experiment

The theory developed in this paper predicts the breakup of a compound thread resulting in the formation of compound drops and gives the linear theory's estimate of the breakup lengths and of the drop sizes at breakup. Hertz & Hermanrud (1983) have done experiments with a compound jet generated using a single nozzle assembly that was filmed as the jet moved in the axial direction. The primary fluid in their experiment was a water-soluble ink and the secondary fluid was a silicone oil. The physical parameters were: $\sigma_2 = 20 \times 10^{-3}\,\mathrm{N\,m^{-1}}$, $\sigma_1 = 52 \times 10^{-3}\,\mathrm{N\,m^{-1}}$, $\mu_2 = \mu_1 = 2 \times 10^{-3}\,\mathrm{kg\,m^{-1}\,s}$, $\rho_2 = \rho_1 = 1000\,\mathrm{kg\,m^{-3}}$, $R_1 = 75 \times 10^{-6}\,\mathrm{m}$, $R_2 = 150 \times 10^{-6}\,\mathrm{m}$, $V = 1.98\,\mathrm{m\,s^{-1}}$. Their observations include pictures of the compound jet as it comes out of the orifice, and the capillary breakup into compound drops. From the pictures it is possible to measure the wavelength(s) of the spatially growing wave, as in figure 6 of their study. For the system parameters, the Weber number is of order 10, so

https://doi.org/10.1017/S0022112000001282 Published online by Cambridge University Press

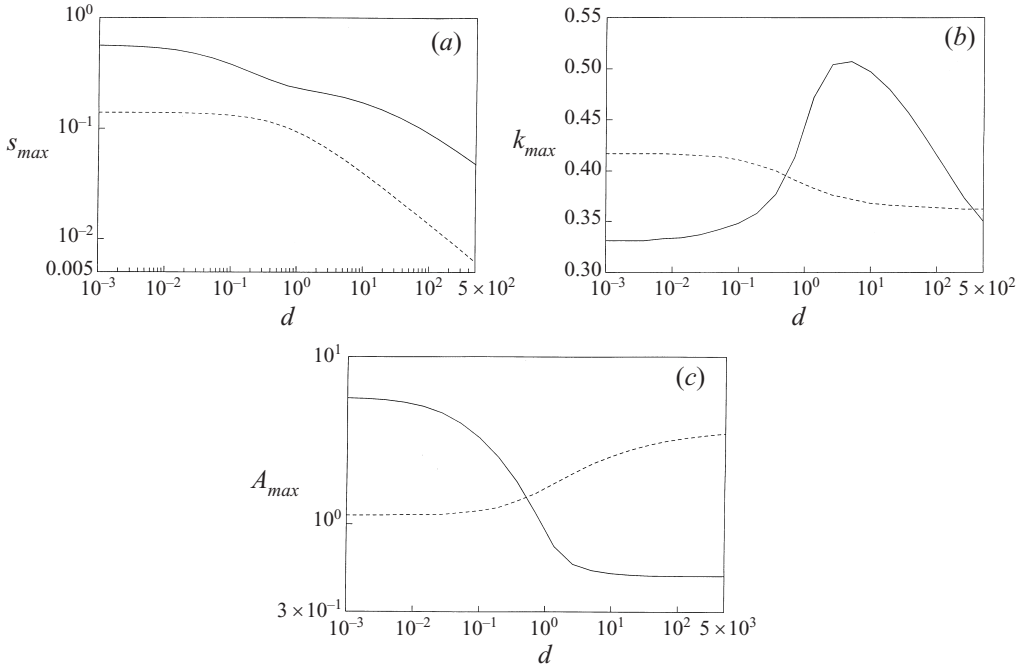


FIGURE 10. Effect of the density ratio d on (*a*) s_{max} (*b*) k_{max}, (*c*) A_{max}. $\gamma = 2$, $a = 2$, $m = 1$, $\boldsymbol{J} = 1000$. ———, Stretching; - - - - -, squeezing.

(as noted in the introduction) we may use the k_{max} from our temporal analysis to predict the wavelength of the observed spatially growing wave. The wavenumber (non-dimensionalized by R_1) from figure 6 of Hertz & Hermanrud (1983) is 0.64 for the first wave. The wavenumber changes in the axial direction and the average is 0.6. Figure 11 shows the predictions of the (non-dimensional) growth rate as a function of the (non-dimensional) wavenumber from our temporal analyses using the physical parameters of the experiment ($\gamma = 0.4$, $d = 1$, $m = 1$, $\boldsymbol{J} = 937$). The maxima in the temporal growth rate is at $k = 0.62$. Sanz & Masseguer (1985) compared the results of the same experiment with their theoretical predictions based on the one-dimensional temporal model. Their prediction for the wavenumber was 0.7, so the inclusion of viscosity and radial motion has brought the linearized theory closer to the experimental results.

We note that the mode with highest growth rate is observable at times sufficiently long that its growth rate dominates all other modes, provided the jet is still in the linear regime. At short times, other modes also contribute and this may explain why the observed wavelength of the jet changes along the axial direction.

6. Discussion and conclusions

A compound thread is unstable due to capillarity. We have solved its temporal linear hydrodynamic stability, and have found two unstable modes. In the stretching mode the interfaces grow in phase, and in the squeezing mode they grow out of phase. The stretching and the squeezing modes are unstable for waves longer than the inner and the outer circumferences, respectively. In the stretching mode, extrapolating the

https://doi.org/10.1017/S0022112000001282 Published online by Cambridge University Press

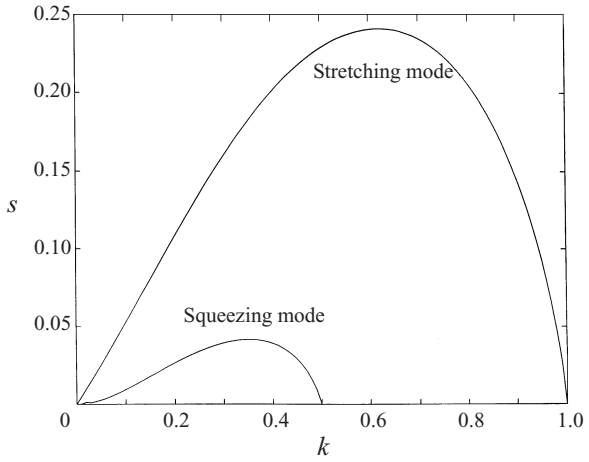


FIGURE 11. Prediction based on the temporal analysis for $\gamma = 0.4$, $a = 2$, $d = 1$, $\boldsymbol{J} = 937$.

growth beyond the linear regime will result (for amplitude ratios of order-one) in the breakup of the core leading to drops of primary fluid in the secondary fluid. If the system continues to follow its pre-breakup dynamics, further nonlinear stretching growth will finally cause rupture of the annular fluid to form compound drops. In the squeezing mode when extrapolating the linear dynamics, either the film or the core can break first depending on the film thickness. In experiments, both modes grow and the one with the higher growth rate will dominate. Our results show that the stretching mode has the higher growth rate, and for most system ratios an amplitude ratio approximately one, and thus dominates the long-time linear regime and the breakup; thus we expect under most conditions compound drops to form. The growth-rate time scales between the two modes become more disparate for thin annular films. In the thin-film limit, the squeezing mode's growth rate goes to zero as ϵ^2. The stretching mode's growth rate goes as ϵ^0 and approaches a single jet with surface tension equal to the sum of the two interfacial tensions.

We present plots of the maximum growth rate, the wavenumber of maximum growth and the amplitude ratio as a function of the ratios of the density and viscosity of the annular to the core fluid, and of the ratio of the surface tension of the outer fluid to the interfacial tension between the outer fluid and the core. Variations in the viscosity, and tension ratios when they have values near one can change k_{max} by a factor of 2 with minimal change in the growth rate or amplitude ratio. The amplitude ratio and the growth rate are most sensitive to changes in the density ratio. These calculations can be used as a guide for understanding how to vary the annular fluid properties to manipulate the breakup length and the drop size of compound jets in technological applications. The formation of compound drops, which is consistent with stretching-mode dominance, was observed by Hertz & Hermanrud (1983). Our predictions of k_{max} compare well with their experiments and provide confidence in using our calculations as guides for predicting jet breakup lengths and drop size.

This work was supported in part by a Petroleum Research Fund grant to DR (ACS-PRF 27403-AC9), a NASA grant to CM (NASA32167), and an Air Force grant to D.P. (F 49620-94-I-0242).

https://doi.org/10.1017/S0022112000001282 Published online by Cambridge University Press

Appendix

The 8×8 matrix introduced in § 2 is given by

$$\begin{pmatrix}
0 & 0 & 0 & 0 \\
kI_1(ka) & kK_1(ka) & kI_1(\beta_2 a) & kK_1(\beta_2 a) \\
I_1(k) & K_1(k) & I_1(\beta_2) & K_1(\beta_2) \\
kI_0(k) & -kK_0(k) & \beta_2 I_0(\beta_2) & -\beta_2 K_0(\beta_2) \\
d\boldsymbol{J}^{1/2} sI_0(ka) + 2mk^2 I_1'(ka) & -d\boldsymbol{J}^{1/2} sK_0(ka) + 2mk^2 K_1'(ka) & 2mk\beta_2 I_1'(\beta_2 a) & 2mk\beta_2 K_1'(\beta_2 a) \\
d\boldsymbol{J}^{1/2} sI_0(k) + 2mk^2 I_1'(k) & -d\boldsymbol{J}^{1/2} sK_0(k) + 2mk^2 K_1'(k) & 2mk\beta_2 I_1'(\beta_2) & 2mk\beta_2 K_1'(\beta_2) \\
2k^2 I_1(ka) & 2k^2 K_1(ka) & I_1(\beta_2 a)(\beta_2^2 + k^2) & K_1(\beta_2 a)(\beta_2^2 + k^2) \\
2mk^2 I_1(k) & 2mk^2 K_1(k) & mI_1(\beta_2)(\beta_2^2 + k^2) & mK_1(\beta_2)(\beta_2^2 + k^2)
\end{pmatrix}$$

$$\begin{pmatrix}
kI_1(k) & kI_1(\beta_1) & -s & 0 \\
0 & 0 & 0 & -s \\
-I_1(k) & -I_1(\beta_1) & 0 & 0 \\
-kI_0(k) & -\beta_1 I_0(\beta_1) & 0 & 0 \\
0 & 0 & 0 & \boldsymbol{J}^{1/2}\gamma(k^2 - 1/a^2) \\
-\boldsymbol{J}^{1/2} sI_0(k) - 2k^2 I_1'(k) & -2k\beta_1 I_1'(\beta_1) & \boldsymbol{J}^{1/2}(1 - k^2) & 0 \\
0 & 0 & 0 & 0 \\
-2k^2 I_1(k) & -I_1(\beta_1)(\beta_1^2 + k^2) & 0 & 0
\end{pmatrix} \tag{A 1}$$

If C_{ij} is the cofactor of $A_{ji}(k, s)$, the cofactor expansion of $\boldsymbol{A}^{-1}(k, s)$ gives, from (19) and (20),

$$\boldsymbol{x}(k, s) = \frac{\boldsymbol{C}(k, s)\boldsymbol{b}(k)}{\det(\boldsymbol{A}(k, s))}. \tag{A 2}$$

Using $\boldsymbol{b}(k)$ from (19) in (A 2), the ith ($i = 1, \ldots, 8$) component of $\boldsymbol{x}(k, s)$ is

$$x_i(k, s) = i\frac{C_{i7}\zeta_{1,0} + C_{i8}\zeta_{2,0}}{\det(\boldsymbol{A}(k, s))}. \tag{A 3}$$

In particular,

$$\zeta_1(k, s) = -\frac{\zeta_{1,0}C_{77}(k, s) + \zeta_{2,0}C_{78}(k, s)}{\det(\boldsymbol{A}(k, s))}, \tag{A 4}$$

$$\zeta_2(k, s) = -\frac{\zeta_{1,0}C_{87}(k, s) + \zeta_{2,0}C_{88}(k, s)}{\det(\boldsymbol{A}(k, s))}. \tag{A 5}$$

One needs to invert (A 3)–(A 5) to get the solution in the space–time domain.

We being by inverting the Laplace transform:

$$\hat{\zeta}_i(k, t) = \frac{1}{2\pi \mathrm{i}} \int_{p(k)-\mathrm{i}\infty}^{p(k)+\mathrm{i}\infty} \zeta_i(k, s)\mathrm{e}^{st}\, \mathrm{d}s, \tag{A 6}$$

where $p(k)$ is real and larger than the largest real part of any singularity of the integrand of (A 6) for that value of k. To perform the line integration, we appeal to the residue theorem. Thus, for a given k, we need to find the poles and branch cuts

https://doi.org/10.1017/S0022112000001282 Published online by Cambridge University Press

of $\zeta_i(k,s)$ in the s-plane. Despite involving $\beta_i = (k^2 + s\boldsymbol{J}^{1/2}d_i/m_i)^{1/2}$, it is easy to show that the integrand has no branch cuts because: (i) β_i only appears in the integrand in combinations which have no branch cuts in the complex s-plane, and (ii) as noted in the text, the logarithmic part of $K_0(\beta_i)$ can be removed exactly from the integrand by elementary row operations. The poles of the integrand in (A 6) can arise from the roots of the dispersion equation, i.e. $\det(\boldsymbol{A}) = 0$, or when the components of the cofactor matrix diverge. For a given $k \neq 0$, this can happen only when β_i becomes 0, i.e. $s = -m_i k^2/(d_i \boldsymbol{J}^{1/2})$. But as $\beta_i \to 0$, asymptotic analysis using $K_0(\beta_i) \sim -\ln(\beta_i)$, $K_1(\beta_i) \sim 1/\beta_i$, $I_0(\beta_i) \sim O(1)$ and $I_1(\beta_i) \sim \beta_i/2$ shows that C_{ij} and $\det(\boldsymbol{A})$ stay finite. Similarly $k = 0$ is not a pole for any s. Thus the only relevant poles $s_n(k)$ of the integrand are those for which $\det(\boldsymbol{A}) = 0$. We evaluate them (a similar expression can be written for ζ_2) assuming they are simple:

$$\hat{\zeta}_i(k,t) = -\sum_n \frac{\zeta_{1,0}C_{77}(k,s_n(k)) + \zeta_{2,0}C_{78}(k,s_n(k))}{\left.\dfrac{\partial \det \boldsymbol{A}}{\partial s}\right|_{k,s_n(k)}} \mathrm{e}^{s_n(k)t}. \tag{A 7}$$

The Fourier inversion requires the initial interfacial disturbances $\zeta_{1,0}$, $\zeta_{2,0}$. If they are periodic and monochromatic, $\zeta_{1,0} = G\mathrm{e}^{\mathrm{i}k_{1,0}z}$, $\zeta_{2,0} = H\mathrm{e}^{\mathrm{i}k_{2,0}z}$ and the Fourier inverse of (A 7) is

$$\zeta_1^{[1]} = -\sum_n \left[GC_{77}[k_{1,0}, s_n(k_{1,0})] \frac{\mathrm{e}^{\mathrm{i}k_{1,0}z + s_n(k_{1,0})t}}{\left.\dfrac{\partial \det \boldsymbol{A}}{\partial s}\right|_{k_{1,0},s_n(k_{1,0})}} \right.$$

$$\left. + HC_{78}[k_{2,0}, s_n(k_{2,0})] \frac{\mathrm{e}^{\mathrm{i}k_{2,0}z + s_n(k_{2,0})t}}{\left.\dfrac{\partial \det \boldsymbol{A}}{\partial s}\right|_{k_{2,0},s_n(k_{2,0})}} \right], \tag{A 8}$$

with a similar expression for $\zeta_2^{[1]}$. An arbitrary periodic initial condition will lead to an outer sum over the poles k_0 of the initial condition. The growth rate s_{max} of the fastest growing mode dominates the long-time solution $\sim \exp(s_{max}t)$, as in normal-mode analysis.

If, rather than being periodic, the initial disturbances are absolutely integrable, their Fourier transforms have no poles on the real k-axis; thus the Fourier integral requires a separate evaluation. Since the integrand of the inversion integral (A 7) grows as $\mathrm{e}^{\mathrm{i}kz + s(k)t}$, we use the method of steepest descent to evaluate its asymptotically long-time limit, where only portions of the domain of integration for which $s_r \geqslant 0$ make non-exponentially small contributions. For k real and positive, s_1 and s_2 are purely real and are shown in figure 3. From the explicit form of the matrix $\boldsymbol{A}$ in (A 1), it is easy to show that k, s real implies $\det(\boldsymbol{A}(k,s)) = \det(\boldsymbol{A}(-k,s))$. Thus $s(k)$ is even. The stretching ($n = 1$) mode contributes for $-1 < k < 1 = k_{c1}$, the squeezing mode ($n = 2$) for $-1/a < k < 1/a = k_{c2}$, and other non-neutral modes decay as $t \to \infty$:

$$\zeta_1^{[1]}(z,t) = -\frac{1}{2\pi} \sum_{n=1}^{2} \int_{-k_{c,n}}^{k_{c,n}} \frac{\zeta_{1,0}C_{77}(k,s_n(k)) + \zeta_{2,0}C_{78}(k,s_n(k))}{\left.\dfrac{\partial \det \boldsymbol{A}}{\partial s}\right|_{k,s_n(k)}} \mathrm{e}^{\mathrm{i}kz + s_n(k)t}\, \mathrm{d}k. \tag{A 9}$$

https://doi.org/10.1017/S0022112000001282 Published online by Cambridge University Press

Note that $s_n(0) = s_n(k_{cn}) = 0$ and $s_n(k)$ goes through a maximum at $0 < k_{mn} < k_{cn}$, where we denote the maximum at k_{mn} by s_{mn}. For each value of n, Watson's lemma (see for example Carrier, Krook & Pearson (1983, chap. 6)) can then be applied separately for the two domains $(0, k_{cn})$ and $(-k_{cn}, 0)$:

$$\zeta_1^{[1]}(z,t) = -\frac{1}{\sqrt{2\pi}} \sum_{n=1}^{2} \frac{\mathrm{e}^{s_{mn}t}}{\sqrt{t}} \left[\mathrm{e}^{\mathrm{i}k_{mn}z} \frac{(\zeta_{1,0}C_{77} + \zeta_{2,0}C_{78})\big|_{k_{mn},s_{mn}}}{[\partial \det \boldsymbol{A}/\partial s]\big|_{k_{mn},s_{mn}} \sqrt{-(\partial^2 s/\partial k^2)\big|_{k_{mn}}}} \right.$$
$$\left. + \mathrm{e}^{\mathrm{i}k_{mn}z} \frac{(\zeta_{1,0}C_{77} + \zeta_{2,0}C_{78})\big|_{-k_{mn},s_{mn}}}{[\partial \det \boldsymbol{A}/\partial s]\big|_{k_{mn},s_{mn}} \sqrt{-(\partial^2 s/\partial k^2)\big|_{k_{mn}}}} \right], \tag{A 10}$$

$$\zeta_2^{[1]}(z,t) = -\frac{1}{\sqrt{2\pi}} \sum_{n=1}^{2} \frac{\mathrm{e}^{s_{mn}t}}{\sqrt{t}} \left[\mathrm{e}^{\mathrm{i}k_{mn}z} \frac{(\zeta_{1,0}C_{87} + \zeta_{2,0}C_{88})\big|_{k_{mn},s_{mn}}}{[\partial \det \boldsymbol{A}/\partial s]\big|_{k_{mn},s_{mn}} \sqrt{-(\partial^2 s/\partial k^2)\big|_{k_{mn}}}} \right.$$
$$\left. + \mathrm{e}^{\mathrm{i}k_{mn}z} \frac{(\zeta_{1,0}C_{87} + \zeta_{2,0}C_{88})\big|_{-k_{mn},s_{mn}}}{[\partial \det \boldsymbol{A}/\partial s]\big|_{k_{mn},s_{mn}} \sqrt{-(\partial^2 s/\partial k^2)\big|_{k_{mn}}}} \right] \tag{A 11}$$

where at k_{mn} it is easy to show from the fact that $\det \boldsymbol{A}(k, s(k)) = 0$ that at k_{mn} $-\partial^2 s/\partial k^2\big|_{k_{mn}} = [\partial^2 \det \boldsymbol{A}/\partial k^2]\big|_{k_{mn},s_{mn}} [\partial \det \boldsymbol{A}/\partial s]^{-1}\big|_{k_{mn},s_{mn}}$ and the second derivative in (A 10) and (A 11) can be replaced by this relation. Thus, the long-time solution depends only on the maxima of the growth rate and recovers the standard $\exp(s_{mn}t)/\sqrt{t}$ form, which differs from the normal mode result by the well known $\sqrt{t}$ in the denominator.

REFERENCES

Basaran, O. A. & Zhang, X. 1995 An experimental study of dynamics of drop formation. *Phys. Fluids* **7**, 1184.

Bechtel, S. E., Carlson, C. D. & Forest, M. G. 1995 Recovery of Rayleigh capillary instability from slender 1-D inviscid and viscous models. *Phys. Fluids* **7**, 2956.

Bogy, D. B. 1978 Use of one-dimensional Cosserat theory to study instability in a viscous liquid jet. *Phys. Fluids* **21**, 190.

Bogy, D. B. 1979 Drop formation in a circular liquid jet. *Ann. Rev. Fluid Mech.* **11**, 207.

Bogy, D. B., Shine, S. J. & Talke, F. E. 1980 Finite difference solution of Cosserat fluid jet equations. *J. Comput. Phys.* **38**, 294.

Bousfield, D. W. & Denn, M. M. 1987 Jet breakup enhanced by an initial pulse. *Chem. Engng Commun.* **53**, 219.

Bousfield, D. W., Stockel, I. H. & Nanivadekar, C. K. 1990 The break-up of viscous jets with large velocity modulations. *J. Fluid Mech.* **218**, 601.

Brenner, M., Shi, X. D. & Nagel, S. R. 1994 Iterated instability during droplet fission. *Phys. Rev. Lett.* **73**, 3391.

Brenner, M. P., Eggers, J., Joseph, K., Nagel, S. R. & Shi, X. D. 1997 Breakdown of scaling in droplet fission at high Reynolds number. *Phys. Fluids* **9**, 1573.

Busker, D. P., Lamers, A. P. & Nieuwenhuizen, J. K. 1989 The nonlinear breakup of an inviscid liquid jet using the spatial instability method. *Chem. Engng Sci.* **44**, 377.

Carrier, G. F., Krook, M. & Pearson, C. E. 1983 *Functions of a Complex Variable: Theory and Technique*. Hod Books, Ithaca, NY.

Chandrasekhar, S. 1961 *Hydrodynamic and Hydromagnetic Stability*. Dover.

Chaudhary, K. C. & Maxworthy, T. 1980*a* The nonlinear capillary instability of a liquid jet. Part 2. Experiments on jet behaviour before droplet formation. *J. Fluid Mech.* **96**, 275.

https://doi.org/10.1017/S0022112000001282 Published online by Cambridge University Press

Chaudhary, K. C. & Maxworthy, T. 1980*b* The nonlinear capillary instability of a liquid jet. Part 3. Experiments on satellite drop formation and control. *J. Fluid Mech.* **96**, 287.

Chaudhary, K. C. & Redekopp, L. G. 1980 The nonlinear capillary instability of a liquid jet. Part 1. Theory. *J. Fluid Mech.* **96**, 257.

Chauhan, A., Maldarelli, C., Rumschitzki, D. & Papageorgiou, D. T. 1996 Temporal and spatial instability of an inviscid compound jet. *Rheol. Acta.* **35**, 133.

Clanet, C. & Lasheras, J. 1999 Transition from dripping to jetting. *J. Fluid Mech.* **383**, 307.

Denn, M. M. 1980 Drawing of liquids to form fibers. *Ann. Rev. Fluid Mech.* **12**, 365.

Donnelly, R. J. & Glaberson, W. 1966 Experiment on capillary instability of a liquid jet. *Proc. R. Soc. Lond.* A **290**, 547.

Eggers, J. 1993 Universal pinching of 3D axisymmetric free surface flow. *Phys. Rev. Lett.* **71**, 3458.

Eggers, J. 1995 Theory of drop formation. *Phys. Fluids* **7**, 941.

Eggers, J. 1997 Nonlinear dynamics and breakup of free-surface flows. *Rev. Mod. Phys.* **69**, 865.

Eggers, J. & Dupont, T. F. 1994 Drop formation in a one-dimensional approximation of the Navier–Stokes equation. *J. Fluid Mech.* **262**, 205.

Goedde, E. F. & Yuen, M. C. 1970 Experiments on liquid jet instability. *J. Fluid Mech.* **33**, 151.

Hertz, C. H. & Hermanrud, B. 1983 A liquid compound jet *J. Fluid Mech.* **131**, 271.

Herzenberg, L. A., Sweet, R. G. & Herzenberg, L. A. 1976 Fluorescence-activated cell sorting. *Sci. Am.* **234**, 108.

Kamphoefner, F. 1972 Ink jet printing. *IEEE Trans. Electron Devices* **ED-19**, 584.

Keller, J. B., Rubinow, S. L. & Tu, Y. O. 1973 Spatial instability of a jet. *Phys. Fluids* **16**, 2052.

Kowalewski, T. A. 1996 On the separation of droplets from a liquid jet. *Fluid Dyn. Res.* **17**, 121.

Lafrance, P. 1975 Nonlinear break up of a laminar liquid jet. *Phys. Fluids* **18**, 428.

Lee, H. C. 1974 Drop formation in a liquid jet. *IBM J. Res. Dev.* **18**, 364.

Leib, S. J. & Goldstein, M. E. 1986*a* Convective and absolute instability of a viscous jet. *Phys. Fluids* **29**, 952.

Leib, S. J. & Goldstein, M. E. 1986*b* The generation of capillary instabilities on a liquid jet. *J. Fluid Mech.* **168**, 479.

Lin, S. P. & Lian, Z. W. 1989 Absolute instability of a liquid jet in a gas. *Phys. Fluids* A **1**, 490.

Mansour, N. & Lundgren, T. S. 1990 Satellite formation in capillary jet breakup. *Phys. Fluids* A **2**, 1141.

McCarthy, J. J. & Molloy, N. A. 1974 Review of the stability of liquid jets and the influence of nozzle design. *Chem. Engng* **7**, 1.

Nayfeh, A. H. 1970 Nonlinear stability of a liquid jet. *Phys. Fluids* **13**, 841.

Papageorgiou, D. T. Maldarelli, C. & Rumschitzki, D. S. 1990 Nonlinear interfacial stability of core annular film flows. *Phys. Fluids* A **2**, 340.

Peregrine, D. H., Shoker, G. & Symon, A. 1990 The bifurcation of liquid bridges. *J. Fluid Mech.* **212**, 25.

Pimbley, W. T. 1976 Drop formation from a liquid jet: a linear one-dimensional analysis considered as a boundary value problem. *IBM J. Res. Dev.* **20**, 148.

Pimbley, W. T. & Lee, H. C. 1977 Satellite droplet formation in a liquid jet. *IBM J. Res. Dev.* **21**, 21.

Radev, S. & Shkadov, V. 1985 On a stability of two-layer capillary jet. *Theor. Appl. Mech.* **16**, 68.

Radev, S. & Tchavdarov, B. 1988 Linear capillary instability of compound jets. *Intl J. Multiphase Flow* **14**, 67.

Rayleigh, Lord 1879 On the instability of jets. *Proc. Lond. Math. Soc.* **10**, 4.

Rutland, D. F. & Jameson, G. J. 1970 Theoretical prediction of the sizes of drops in the breakup of capillary jets. *Chem. Engng Sci.* **25**, 1689.

Rutland, D. F. & Jameson, G. J. 1971 A nonlinear effect in the capillary instability of liquid jets. *J. Fluid Mech.* **46**, 267.

Sanz, A. & Masseguer, J. 1985 One-dimensional linear analysis of the compound jet. *J. Fluid Mech.* **159**, 55.

Schulkes, R. M. S. M. 1993 Dynamics of liquid jets revisited. *J. Fluid Mech.* **250**, 635.

Shi, X. D., Brenner, M. P. & Nagel, S. R. 1994 A cascade of structure in a drop falling from a faucet. *Science* **265**, 219.

https://doi.org/10.1017/S0022112000001282 Published online by Cambridge University Press

Shkadov, V. Y. & Sisoev, G. M. 1996 Instability of a two layer capillary jet. *J. Multiphase Flow* **22**, 363.

Taub, H. H. 1976 Investigation of nonlinear waves on liquid jets. *Phys. Fluids* **19**, 1124.

Ting, L. & Keller, J. B. 1990 Slender jets and thin sheets with surface tension. *SIAM J. Appl. Maths* **50**, 1533.

Tjahjadi, M., Stone, H. A. & Ottino, J. 1992 Satellite and subsatellite formation in capillary breakup. *J Fluid Mech.* **243**, 297.

Tomotika, S. 1935 On the instability of a cylindrical thread of a viscous liquid surrounded by another viscous liquid. *Proc. R. Soc. Lond.* A **150**, 322.

Vassallo, P. & Ashgriz, N. 1991 Satellite formation and merging in liquid jet breakup. *Proc. R. Soc. Lond.* A **433**, 269.

Wang, D. P. 1968 Finite amplitude effect on the stability of a jet of circular cross-section. *J. Fluid Mech.* **34**, 299.

Wilson, S. D. R. 1988 The slow dripping of a viscous liquid. *J. Fluid Mech.* **190**, 561.

Yarin, A. L. 1993 *Free Liquid Jets and Films: Hydrodynamic and Rheology*. Longman.

Yuen, M. C. 1968 Non-linear capillary instability of a liquid jet. *J. Fluid Mech.* **33**, 151.

Zhang, D. & Stone, H. A. 1997 Drop formation in viscous flows at a vertical capillary tube. *Phys. Fluids* **9**, 2234.

Zhang, X. 1999 Dynamics of growth and breakup of viscous pendant drops in air. *J. Colloid Interface Sci.* **212**, 107.

https://doi.org/10.1017/S0022112000001282 Published online by Cambridge University Press